Modification of aerosol mass and size distribution due to aqueous-phase SO_2 oxidation in clouds: Comparisons of several models

Sonia M. Kreidenweis,[1] Chris J. Walcek,[2] Graham Feingold,[3] Wanmin Gong,[4] Mark Z. Jacobson,[5] Cheol-Hee Kim,[6] Xiaohong Liu,[7] Joyce E. Penner,[7] Athanasios Nenes,[8,9] and John H. Seinfeld[8]

Received 25 June 2002; revised 20 September 2002; accepted 27 November 2002; published 8 April 2003.

[1] Models of aerosol scavenging and aqueous-phase oxidation of SO_2 by H_2O_2 and O_3 in a cloud updraft are compared. Bulk models considering only a single droplet size are compared with size-resolved models that explicitly simulate multiple aerosol and drop sizes. All models simulate growth of cloud drops on a lognormal ammonium bisulfate aerosol distribution, and subsequent aqueous-phase chemistry during adiabatic ascent. In agreement with earlier published studies, it is found that relative to bulk models, the size-resolved cloud chemical models consistently calculate 2–3 times more oxidation via the $SO_2 + O_3$ pathway, due to calculated variability of cloud water pH among cloud drops. All models calculate high scavenging of the input dry aerosol mass, but the calculated number of cloud drops formed varies from 275–358 drops cm^{-3}. Differences in the calculated number of cloud drops formed result from the treatment of gaseous species uptake, solution thermodynamics, applied water condensation mass accommodation coefficient, and bin size range definitions over which the input aerosol distribution is numerically approximated. The difference in calculated cloud drop number can under many conditions propagate to appreciable variations in cloud albedo. It is found that the modifications to the aerosol size and mass spectrum are sensitive to the number of cloud drops formed, and differences in the processed aerosol spectra were found to induce up to 13% differences in calculated light extinction properties of the modified particle distributions. These significant discrepancies among cloud aerosol chemistry interaction models, even when used to simulate relatively simple conditions, suggest that parameterizations of these processes used in larger-scale cloud, regional and longer-term climate models can contain high levels of uncertainty. *INDEX TERMS:* 0305 Atmospheric Composition and Structure: Aerosols and particles (0345, 4801); 0320 Atmospheric Composition and Structure: Cloud physics and chemistry; 0317 Atmospheric Composition and Structure: Chemical kinetic and photochemical properties; 0365 Atmospheric Composition and Structure: Troposphere—composition and chemistry; 0368 Atmospheric Composition and Structure: Troposphere—constituent transport and chemistry; *KEYWORDS:* aerosol size distribution, aqueous chemistry, sulfur oxidation, cloud chemistry

Citation: Kreidenweis, S. M., C. J. Walcek, G. Feingold, W. Gong, M. Z. Jacobson, C.-H. Kim, X. Liu, J. E. Penner, A. Nenes, and J. H. Seinfeld, Modification of aerosol mass and size distribution due to aqueous-phase SO_2 oxidation in clouds: Comparisons of several models, *J. Geophys. Res.*, *108*(D7), 4213, doi:10.1029/2002JD002697, 2003.

1. Introduction

[2] Atmospheric particles containing sulfate are a dominant component of acidic deposition, and also contribute to fine particle pollution associated with regional haze [*Malm et al.*, 1994] and health problems [*Health Effects Institute*, 2000]. Also, sulfate aerosol pollution induces an appreciable radiative cooling impact on global climate that

[1]Department of Atmospheric Science, Colorado State University, Fort Collins, Colorado, USA.
[2]Atmospheric Science Research Center, State University of New York, Albany, New York, USA.
[3]National Oceanographic and Atmospheric Administration, Boulder, Colorado, USA.
[4]Meteorological Service of Canada, Downsview, Ontario, Canada.
[5]Department of Civil and Environmental Engineering, Stanford University, Palo Alto, California, USA.
[6]National Institute of Environmental Research (NIER), Seo-gu, Incheon, Korea.
[7]Atmospheric, Oceanic and Space Sciences, University of Michigan, Ann Arbor, Michigan, USA.
[8]Division of Chemistry and Chemical Engineering, California Institute of Technology, Pasadena, California, USA.
[9]Now at School of Earth and Atmospheric Sciences, Georgia Institute of Technology, Atlanta, Georgia, USA.

0148-0227/03/2002JD002697$09.00

counters the potential CO_2-induced warming influences, but considerable uncertainties persist about quantifying the direct and indirect radiative effects of sulfate aerosols on climate [*Intergovernmental Panel on Climate Change*, 2001].

[3] Sulfate is a significant and frequently the dominant component of aerosol mass in the atmosphere, and is produced primarily from the oxidation of SO_2. This oxidation occurs in the gas phase through reaction with the hydroxyl radical, and the characteristic rate of the gas-phase reaction is on the order of a few percent per hour during the day [*Stockwell et al.*, 1990]. In cloudy environments containing sufficient oxidants, SO_2 is rapidly oxidized by aqueous reactions with hydrogen peroxide, ozone, organic peroxides and a number of other oxidants. It is generally recognized that the dominant mechanism of sulfate formation in the troposphere is via reactions of SO_2 with H_2O_2 and O_3 in clouds [*Walcek and Taylor*, 1986; *Barth et al.*, 2000; *Rasch et al.*, 2000]. Therefore it is important for atmospheric models that include sulfate to simulate accurately the oxidation of SO_2 in clouds. Most larger-scale models of atmospheric sulfur simulate in-cloud SO_2 oxidation using a simplified "bulk" modeling approach, where oxidation rates are calculated using a single characteristic water content, droplet size and acidity level [e.g., *Chang et al.*, 1987; *Iribarne and Cho*, 1989].

[4] The aqueous-phase addition of mass to particles has direct and indirect radiative effects. Because of the global importance of sulfur gases and sulfate aerosol, this species has been the focus of the most study in the literature. The direct radiative effects are sensitive to the details of the initial aerosol distribution and how mass is added to the aerosol spectrum [e.g., *Lelieveld and Heintzenberg*, 1992; *Hegg et al.*, 1996]. In turn, aqueous chemistry depends on the cloud drop spectrum. Indirect radiative effects arise from variations in drop spectra induced by changes in the input aerosol, and subsequent changes in cloud albedo. The concept of susceptibility of warm clouds to such albedo changes was first proposed by *Twomey* [1991], and later studies focused specifically on the link between sulfate aerosols, cloud condensation nuclei, and cloud droplet spectra in indirect radiative effects [e.g., *Hegg*, 1994; *Jones et al.*, 1994; *Boucher and Lohmann*, 1995].

[5] Here several bulk and size-resolved aerosol/cloud/chemistry models are compared under a well-defined set of conditions in order to assess the uncertainties associated with different modeling approaches. The results presented here summarize the findings of the aerosol parcel model component of the World Meteorological Organization 5th International Cloud Modeling Workshop held in Glenwood Springs, Colorado, United States, in August 2000. The problem statement was first designed and disseminated in early 2000, and discussions and revisions of results continued before and after the August 2000 workshop.

2. Models Compared

[6] Seven participating modeling groups submitted twelve simulations for comparison. Table 1 identifies the models divided into simpler bulk models and more sophisticated, size-resolved models. The five groups contributing size-resolved calculations also submitted bulk versions of their models, and two groups contributed only bulk calculations. In subsequent figures, each model is identified using the first letter of the name identified on Table 1, and model results are further identified as "bulk" or "size-resolved." Many of the cloud chemistry models used here are extracted from larger-scale atmospheric models, and the references to related applications are listed in the right column of Table 1.

Table 1. Summary of Participating Models

Name (Institution)	Bulk Model	Size-Resolved (Number Sizes)	References
Feingold (NOAA/ETL)	x	20	*Feingold et al.* [1998]
Gong (MSC)	x	20	*Gong* [2002]
Jacobson (Stanford)	x	50	*Jacobson* [2002]
Liu (Michigan)	x	30	*Liu and Seidl* [1998]
Nenes (CalTech)	x	60	*Nenes et al.* [2001]
Kim (CSU)	x		*Kim et al.* [2002]
Walcek (SUNY)	x		*Walcek and Taylor* [1986]

[7] Further characteristics of the size-resolved models are summarized in Table 2. All of the models employ a so-called "discrete, Lagrangian" or "moving bin" approach. Although the models represent the aerosol and drop spectra as moving (in size space), discrete points, we will use the term "bin" here when discussing these points. All of the size-resolved models also solve gas-liquid transfer simultaneously with aqueous chemistry, and all treat this transfer as a nonequilibrium process.

[8] All models used the identical simulation conditions presented in the next section, and differences between the models arise from different numerical integration methods, different aerosol and droplet size resolutions used by the size-resolved models, and different methods for assessing cloud drop activation and water activity. In addition, the transfer of soluble HNO_3 and NH_3 gases before and during droplet growth influences the growth calculations for the size-resolved models.

3. Comparison Conditions

[9] All models calculate the aqueous chemical composition of cloud water within a cloud updraft. Dissolved constituents in cloud water result from the scavenging of a specified lognormal dry aerosol size distribution and dissolution of gases, and concentrations are modified by the oxidation of SO_2 by H_2O_2 and O_3. The physical conditions simulated are listed in the top half of Table 3. The chemical composition of cloud water is simulated for an air parcel lifted adiabatically at 0.5 m s^{-1} starting from a height slightly below cloud base. Cloud base is reached 196 s into the simulation, and simulations continue for an additional 2400 s (1.2 km) above cloud base. At the end of the simulation, the cloud water is evaporated and the resulting dry aerosol distributions are compared.

[10] The relatively unpolluted chemical conditions chosen for the simulation are listed in the bottom portion of Table 3. The initial ammonium and sulfate concentrations represent a slightly acidic ammonium bisulfate aerosol. The initial ammonia gas concentration is present in excess with respect to equilibrium with this aerosol composition, which can have consequences for aerosol-cloud interactions [*Seidl*, 1989], as

Table 2. Characteristics of Size-Resolving Models

	Feingold	Gong	Jacobson	Liu	Nenes
Bin structure	moving discrete	Lagrangian, remapped to initial grid	moving discrete	moving discrete	moving discrete
Numerical solver	gear-type (VODE)	Young-Boris hybrid predictor- corrector	gear-type (SMVGEAR II)	McRae solver (semi-implicit method)	gear-type (VODE)
Maximum time step	2 s	0.2 s	900 s (not reached)	0.2 s	0.02 s
Number of size bins	20	20	50	30	60
Start of aqueous chemistry	Conc < 2 M	at activation	prior to activation	prior to activation	prior to activation
Influence of gas uptake on activation	none; initial composition is assumed	none; activation is parameterized according to critical radius for input distribution	NH_3 and HNO_3 taken up before activation, but not re-equilibrated before start	uptake of gases before activation allowed; initial re-equilibration with gas-phase NH_3 performed	NH_3 and HNO_3 are taken up before activation, but not re-equilibrated before start of run
Aerosol liquid water content	ZSR, using binary data from known ammoniated sulfate solutions, for both aerosols and drops	not computed	ZSR for aerosol; for drops, Köhler equations used, computing ν from number of ions, but setting osmotic coefficient to 1	Köhler equations used, computing ν from ion number, osmotic coefficient set to 1	Köhler equations used, computing ν from number of ions, but setting osmotic coefficient to 1
Bin activation	entire bin activated at once	Partial bin activation allowed	Entire bin activated at once	Entire bin activated at once	Entire bin activated at once
Water condensation accommodation coefficient	0.042	N/A	0.5	1.0	1.0
Droplet number concentration at cloud base (cm^{-3}, initial T and P)	310	283	275	358	301

discussed in section 5. Initial H_2O_2 and O_3 concentrations are well in excess of SO_2 available for oxidation.

[11] The initial number of particles per cm^3 (N) is defined as a function of particle diameter D, using a lognormal, monomodal dry aerosol size distribution where

$$\frac{dN}{d(\ln D)} = \frac{N_T}{\sqrt{2\pi}\ln(\sigma_g)} \exp\left[-\frac{\left[\ln(D) - \left(D_g\right)\right]^2}{2\left[\ln(\sigma_g)\right]^2}\right]. \quad (1)$$

The median diameter $D_g = 0.08$ μm, the geometric standard deviation $\sigma_g = 2$, and the total aerosol number concentration $N_T = 566$ cm^{-3}. A dry particle density of 1.8 g cm^{-3} is assumed. Input mass and number concentrations expressed in absolute concentration units (μg m^{-3}, particles cm^{-3}) are defined at the initial (t = 0) temperature and pressure listed in Table 3. The assumption of a monomodal, single-composition aerosol is made in order to deal with as simple a system as possible when diagnosing differences among models. Many previous studies have been initialized with more realistic bimodal and externally mixed aerosol distributions and have found that model predictions vary with the relative sizes and compositions of the two modes [e.g., *Ayers and Larson*, 1990; *Hegg et al.*, 1992; *Yuen et al.*, 1994; *Hoppel et al.*, 1994; *Hegg et al.*, 1996].

[12] All models use the identical aqueous-phase equilibria listed in Table 4. Oxidation of SO_2 by O_3 and H_2O_2 in the cloud water is specified using the pH-dependent reaction formulations and temperature dependencies shown in Table 5. The ozone reaction varies inversely with approximately the square of the H^+ concentration, while the H_2O_2 reaction is largely insensitive to pH.

4. Sulfur Chemistry

[13] Figure 1 shows the general meteorological and chemical conditions of the parcel as it rises. Figure 1a shows a nearly linear increase in condensed liquid water content above cloud base. All models calculate that 75–80% of the initial SO_2 is oxidized to sulfate during the 40 min

Table 3. Cloud Conditions

Factor	Value (Units)
Physical Conditions	
Height above surface at time = 0	600 (m)
Temperature at t = 0	285.2 (K)
Relative humidity at t = 0	95 (%)
Pressure at t = 0	950 (mbar)
Cloud base height above surface	698 (m)
Cloud base pressure	939 (mbar)
Cloud base temperature	284.2 (K)
Air density at cloud base	1.15 (kg m^{-3})
Updraft velocity	0.5 (m s^{-1})
Cloud water mixing ratio 1200 m (2400 s) above cloud base	2.17 (g kg^{-1})
Chemical Conditions	
SO_2 at t = 0	200 (ppt-v)
NH_3(g) at t = 0	100 (ppt-v)
H_2O_2 at t = 0	500 (ppt-v)
HNO_3 at t = 0	100 (ppt-v)
O_3 at t = 0	50 (ppb-v)
CO_2 at t = 0	360 (ppm-v)
$SO_4^=$ (particulate) at t = 0	2 (μg m^{-3})
NH_4^+ (particulate) at t = 0	0.375 (μg m^{-3})

Table 4. Aqueous-Phase Equilibria

Equilibrium	K_{298}[a]	$-\Delta H/R$[b]	Accommodation Coefficient
$O_3(g) \Longleftrightarrow O_3(aq)$	1.13×10^{-2}	2540	0.00053
$H_2O_2(g) \Longleftrightarrow H_2O_2(aq)$	7.45×10^{4}	7300	0.018
$HNO_3(g) \Longleftrightarrow HNO_3(aq)$	2.1×10^{5}	-[c]	0.05
$CO_2(g) \Longleftrightarrow CO_2(aq)$	3.4×10^{-2}	2440	0.05
$SO_2(g) \Longleftrightarrow SO_2(aq)$	1.23	3150	0.035
$NH_3(g) \Longleftrightarrow NH_3(aq)$	62	4110	0.05
$H_2O_2(aq) \Longleftrightarrow HO_2^- + H^+$	2.2×10^{-12}	−3730	
$CO_2(aq) \Longleftrightarrow HCO_3^- + H^+$	4.3×10^{-7}	−1000	
$HCO_3^- \Longleftrightarrow CO_3^{2-} + H^+$	4.68×10^{-11}	−1760	
$SO_2(aq) \Longleftrightarrow HSO_3^- + H^+$	1.3×10^{-2}	1960	
$HSO_3^- \Longleftrightarrow SO_3^{2-} + H^+$	6.6×10^{-8}	1500	
$NH_3(aq) \Longleftrightarrow NH_4^+ + OH^-$	1.7×10^{-5}	−450	
$HNO_3(aq) \Longleftrightarrow NO_3^- + H^+$	15.4	8700[c]	

[a]Units of K are moles $liter_{(water)}^{-1}$ atm^{-1} or moles $liter_{(water)}^{-1}$.
[b]Equilibrium for other temperatures (T) calculated as $K(T) = K_{298} \exp[-\Delta H/R(1/T-1/298)]$.
[c]Value for $HNO_3(g) \Longleftrightarrow NO_3^- + H^+$.

simulation (Figure 1b). In Figures 1a and 1b, the solid black and the gray lines denote the maximum and minimum of the range of quantities calculated by the 12 models.

[14] Figure 1c shows the calculated water-mass-weighted average cloud water pH as a function of distance above cloud base according to the models. Again, the two curves in Figure 1c denote the range of the 12 models' calculations. Due to the low water content near cloud base, and the acidic nature of the aerosols, cloud water pH starts off very low, less than pH 3.6, but rapidly increases as the acidic material is diluted with increasing amounts of condensing water. Although ammonia gas is absorbed during the initial stages of cloud formation, HNO_3 is also absorbed, so that the observed increase in pH is due primarily to the effects of dilution. All models calculate that greater than 97% of the initial dry aerosol mass is incorporated into the cloud water.

[15] Figure 2 plots the calculated total sulfate production as a function of the liquid-water-weighted pH 1.2 km above cloud base, showing approximately 20% range in the calculated sulfate production, and a corresponding deviation in the calculated acidity $[H^+]$ in the cloud water. The thick gray line in Figure 2 shows the slope of relationship between pH and sulfate assuming H^+ is linearly related to sulfate concentration in the cloud water. This figure clearly shows that the size-resolved models disagree significantly from the bulk models, and calculate about 17% more sulfate production, leading to higher acidity and thus slightly lower cloud-water-averaged pHs. The seven bulk models agree with each other to ±4%, slightly larger than the discrepancies of the five size resolved models (±3%).

[16] Figure 3 provides a further breakdown of the calculated SO_2 oxidation showing the sulfate produced by O_3 and via H_2O_2, plotted against each other. Here there is a distinct clustering of most of the size-resolved models showing about 45 parts per trillion (ppt) more (a factor of 2–3 more) sulfate formation via the pH-dependent O_3 pathway relative to the bulk models, which consistently calculate about 30 ppt sulfate production via O_3 oxidation. This extra sulfate production from ozone by the size-resolved models is somewhat countered by a decrease in sulfate formation from H_2O_2, which is about 20–25 ppt less in the size resolved models relative to the bulk models. Generally there is an inverse relationship between the magnitude of the H_2O_2 versus O_3 oxidation: As more sulfate is produced via the O_3 reaction, less SO_2 is available for the H_2O_2 reaction, and sulfate production from H_2O_2 decreases. Therefore the size-resolved models calculate less sulfate production via the H_2O_2 pathway, even though this reaction rate is largely independent of pH.

[17] Figures 2 and 3 demonstrate that there is a systematic and significant difference between the calculations of aqueous-phase SO_2 oxidation by bulk and size-resolved models of cloud water chemistry, as has been shown previously [e.g., *Hegg and Larson*, 1990; *Gurciullo and Pandis*, 1997; *Ogren and Charlson*, 1992]. This results primarily from the strong pH dependence of the aqueous-phase reaction between SO_2 and O_3 in cloud water, and the pH differences that can exist among numerous drop categories in a cloud. Any differences in pH among cloud droplets will lead to different average rates of the reaction between SO_2 and O_3 in clouds.

[18] Figure 4 shows examples of the calculated distribution of pH among the cloud water mass 1.2 km above cloud base according to three of the size-resolved aqueous chemistry models. In this figure, the pH of each liquid water fraction is plotted cumulatively, and the liquid-water-weighted average pH is shown below each model label. In all models, cloud drops forming on smaller aerosols are calculated to have a higher pH, and the largest activated aerosols grow into the most acidic cloud drops. Figure 4 shows that the Gong and Liu models have a small fraction of their water mass (10%–20%) with the highest pH ($\geq$5.2), despite calculating a more acidic average pH. In contrast, the less acidic Jacobson model contains no water with pH >5.2. Since the ozone oxidation rate is approximately inversely proportional to the square of the H^+ concentration in cloud water, a change in 1 pH point represents a ~100-fold change in the reaction rate of SO_2 and O_3 in cloud water. A doubling of the $SO_2 + O_3$ oxidation rate requires only a 0.3 pH point increase. The Gong and Liu size-resolved models calculate appreciably greater SO_2 oxidation than the Jacobson model, primarily because appreciable fractions of the cloud water have a higher pH than the highest pH calculated by Jacobson's model. Despite these

Table 5. Aqueous-Phase Reactions

Reaction	Rate Expression[a]	k_{298}	$-E/R$
$O_3 + SO_2(aq) \Rightarrow S(VI)$[b]	$k_{298}\exp[-E/R(1/T-1/298)]$	2.4×10^{4}	0
$O_3 + HSO_3^- \Rightarrow S(VI)$[b]	$k_{298}\exp[-E/R(1/T-1/298)]$	3.5×10^{5}	−5530
$O_3 + SO_3^{2-} \Rightarrow S(VI)$[b]	$k_{298}\exp[-E/R(1/T-1/298)]$	1.5×10^{9}	−5280
$H_2O_2(aq) + HSO_3^- \Rightarrow S(VI)$[b]	$\frac{k_{298}[H^+]\exp[-E/R(1/T-1/298)]}{1+13[H^+]}$	7.45×10^{7}	−4430

[a]Units of k are $liter_{(water)}$ $moles^{-1}$ s^{-1}.
[b]$S(VI) = SO_4^{2-} + HSO_4^-$.

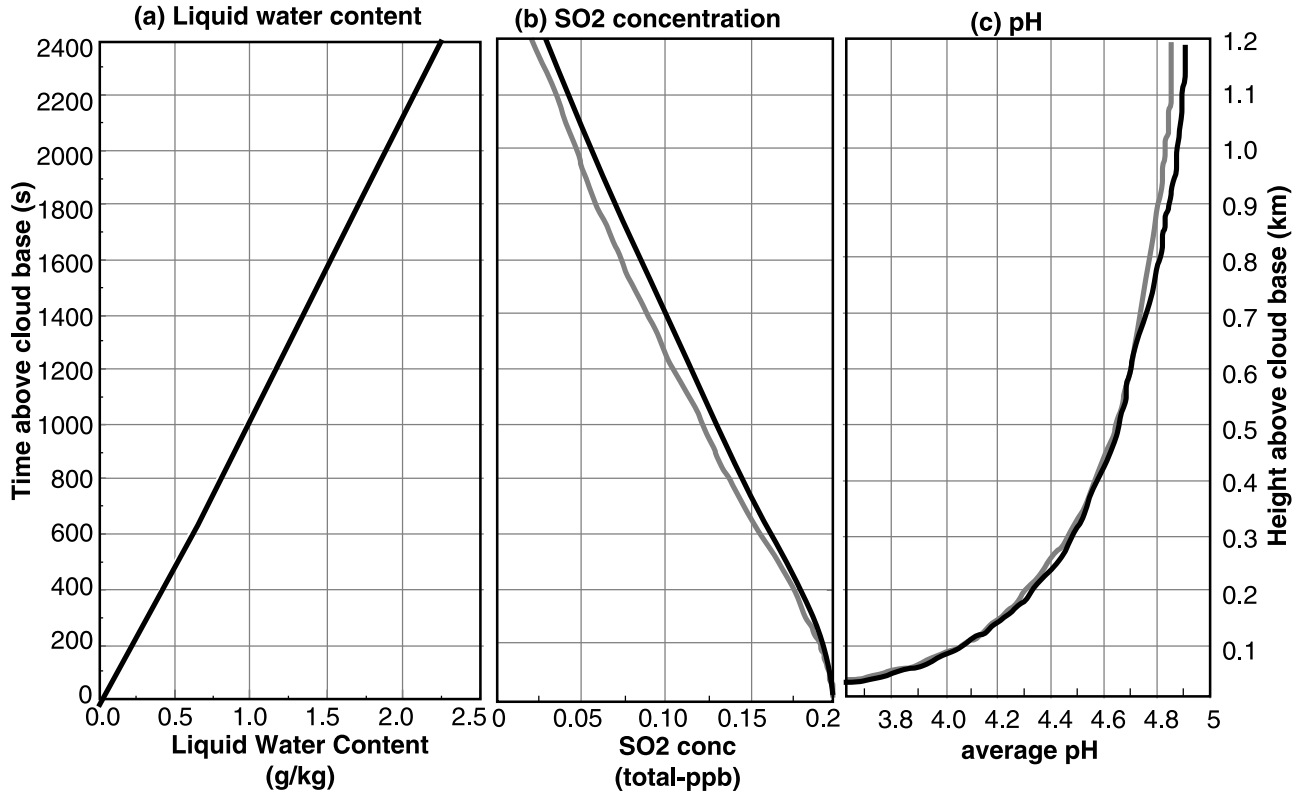

Figure 1. Vertical variation of various meteorological and chemical factors in cloud updraft according to models considered in this study. (a) Condensed liquid water mixing ratio. (b) Total gas + aqueous SO_2 concentration. (c) Average cloud water pH. Simulation starts 196 s (~0.1 km) below cloud base and continues for 2400 s (1.2 km) above cloud base. Grey and black lines denote lower and upper bounds of values calculated by models use in this study.

considerable ranges and differences, the average pH calculated by the size-resolved models agrees to within 0.03 pH units (Figure 1).

5. Cloud Drop Number Concentrations and Modification of Aerosol Size Distributions

[19] The number concentration of cloud droplets computed in each of the five size-resolved models is shown in the last row of Table 2, from 275 cm^{-3} for Jacobson's model to 358 cm^{-3} for Liu's model. This variation can be traced to a number of assumptions made in the models. Although, as shown in Table 2, different numerical solvers are used in the models, we did not find any appreciable differences in results that could be traced to the solvers, but found that other factors were important. First, while the Feingold, Jacobson, Liu, and Nenes models explicitly treat the growth of droplets by water condensation and calculate the time history of ambient water saturation ratio, the Gong model uses a parameterization as implemented in the regional model AURAMS [*Gong*, 2002]. This parameterization is based on a simple empirical relation between the number density of cloud condensation nuclei (and thus cloud drops) and that of the ambient atmospheric aerosols [*Jones et al.*, 1994]. The largest particles are assumed to activate first; the smallest size of "activated" particle is determined by counting downward from the large end of the aerosol spectrum until the specified total number of CCN is accumulated. The adiabatic liquid water content, computed from thermodynamic considerations alone, is distributed evenly among the "activated" particles to determine drop size, resulting in a relatively narrow cloud droplet spectrum. Differences in drop size arise only at the large end of the drop spectrum, and originate from the chosen step size for updating LWC (60 s for this study). Despite the simplicity of this treatment, the number of drops computed in the Gong model is similar to that computed by the other models.

[20] Differences between the Feingold, Jacobson, Liu and Nenes models derive from a number of factors. The water condensation mass accommodation coefficient (α) used in each model is shown in Table 2, and varies from 0.042 to 1. The higher the applied value of α, the more effective is condensational growth at scavenging water vapor that would otherwise go toward activation of more droplets. The corresponding variation in droplet number concentration (N_D) is shown in Figure 5, where Feingold, Liu and Nenes varied the value of α from 1 to 0.042, resulting in 12–35% increases in N_D. The relationship between droplet number concentration (N_D) and maximum supersaturation for the Feingold, Jacobson, Liu and Nenes models, using the base-case values of α assumed in each as indicated on the plot, is shown in Figure 6. From this figure it is apparent that differences in treatment of water condensation cannot alone account for the differences in predicted drop number concentrations, since there should be a positive, monotonic

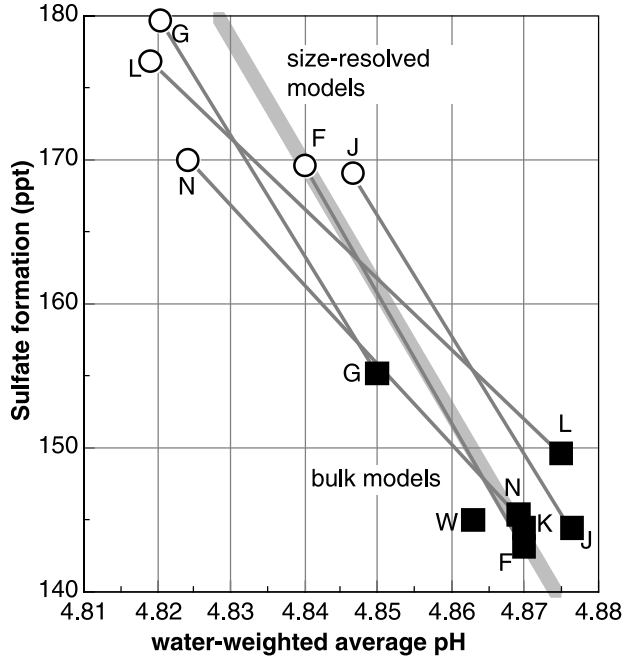

Figure 2. Calculated net sulfate formation plotted against cloud water pH after parcel lifted 1.2 km above cloud base according to all models. Filled squares denote bulk aqueous chemistry models. Open circles denote size-resolved aerosol/cloud water models. Gray line denotes the slope of the pH-sulfate relationship assuming H^+ is proportional to total sulfate. Letters next to each point refer to the first letter of the contributing model shown in Table 1. Fine stippled lines connect models of the same authors.

relationship between S_{max} and N_D with decreasing α. Those models using $\alpha = 1$ (Nenes and Liu) did compute the lowest maximum supersaturation (S_{max}), but predicted higher number concentrations than the other models. The reasons for these differences are twofold: First, the droplet solution thermodynamics is treated differently among these models, and second, each model has a different bin structure. This affects the calculated N_D because none of these models treats activation of partial bins.

[21] None of the models adjusted chemical reactions (except gas-liquid equilibria, and reversible liquid-liquid equilibria in the Jacobson model) for nonideal conditions under high ionic strengths. The Feingold model does not allow for transfer of gases or chemical reaction until droplets are sufficiently dilute (ionic strength <2 M). Thus the water content of drops before activation is based primarily on the initial aerosol composition. During all phases of aerosol and drop growth, the water vapor pressure over the drop is computed from a Köhler-type equation, but without the dilute approximation. Drop size is solved for iteratively, using water activity as a function of composition from the ZSR relationship, and using binary ammoniated sulfate solution data from *Tang and Munkelwitz* [1994]. The Jacobson, Liu, and Nenes models use the Köhler equations with the dilute approximation to compute droplet size, with the number of ions, ν, set according to the evolving composition of the drops. These latter three models all permit gas transfer to the aqueous phase from the start of the simulation, so the aerosol in general contains more soluble material than the initial conditions suggest and is therefore easier to activate, tending to produce higher N_D. This explanation was confirmed by Nenes, who found drop number concentrations of 290 cm^{-3} when uptake of gases was ignored, compared with 301 cm^{-3} when gas transfer prior to and during activation was included. In addition, the Liu model re-equilibrates the aerosol composition with the specified initial ammonia gas concentration, so that this case has essentially a different input aerosol spectrum that leads to significantly larger N_D. This interpretation was borne out by a sensitivity study performed by *Jacobson* [2002], wherein he re-ran his model with the same initial re-equilibration assumption as used by *Liu and Seidl* [1998] and computed 321 drops cm^{-3}, compared with 275 drops cm^{-3} in the model run without this assumption.

[22] The grids that are used by the various size resolving models also play a role in determining the number concentration of droplets. Figure 7 shows the superposition of initial dry aerosol size distribution, approximate critical supersaturation for this spectrum, and "bin" structure for the five size-resolved models (arbitrary y axis). The range of S_{max} predicted by the models is indicated by the shaded region, and corresponds to particles with diameters from about 0.055–0.087 μm. Since the maximum supersaturations fall near the peak of the aerosol size distribution, it is clear that small deviations in predicted S_{max} will translate into relatively large changes in N_D. Cumulative number concentrations (computed from the large end of the spectrum) vary from 375 to 235 cm^{-3} between these diameters; the models have 2–4 "bins" across this range. Thus, depending on the

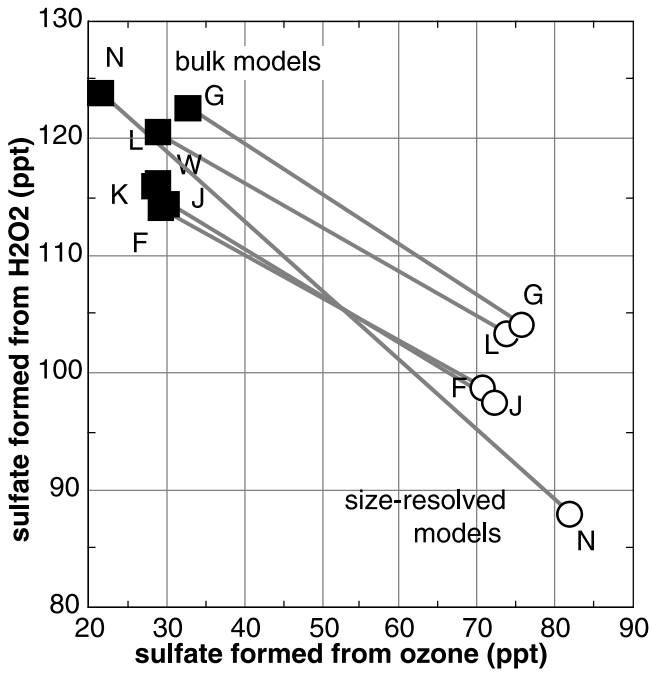

Figure 3. Cumulative sulfate formation via H_2O_2 versus sulfate formation via O_3 at 1.2 km above cloud base. Filled squares denote bulk aqueous chemistry models. Open circles denote size-resolved aerosol/cloud water models. Letters next to each point refer to the first letter of the contributing model shown in Table 1. Fine stippled lines connect models of the same authors.

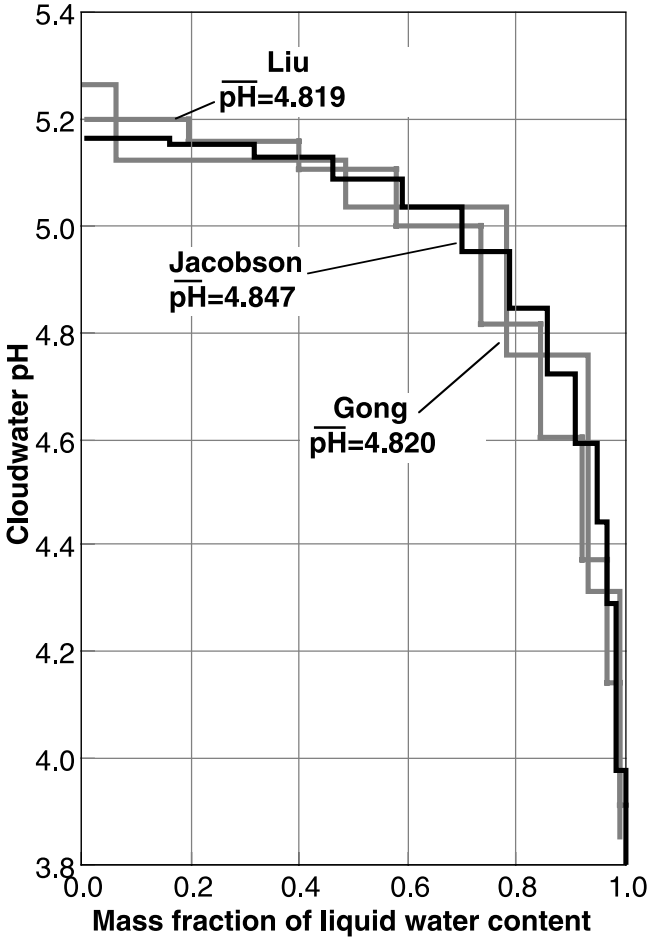

Figure 4. The pH of various fractions of the liquid water mass in cloud updraft according to three size-resolved models (listed in Table 1) 1.2 km above cloud base. Water-weighted average pH is noted under each model name.

model size resolution, if the predicted S_{max} falls just inside or just outside one of the "bins", a difference of 30 or more droplets cm^{-3} can be computed, since these models treat the contents of each "bin" as represented by a single size particle. The effects of resolution on predicted N_D are explored further in Figure 8. In most (but not all) cases, N_D decreased when resolution was increased, suggesting that S_{max} was falling just inside a relatively large bin in the base cases. However, it is difficult to generalize the relationship between N_D and size resolution, since it depends on the maximum supersaturation, the aerosol size distribution, and the setup of the grid in diameter space.

[23] Figures 9a–9e show the modifications to the dry sulfate aerosol mass distribution calculated by the five size-resolved models. The cloud drops 1.2 km above cloud base are evaporated, and the resulting dry aerosol size distributions are compared with the initial input spectrum. Within the cloud updraft, dry aerosols are activated in the lowest several tens of meters above cloud base, and all models activate from the largest aerosols down to a cutoff size determined by the simulated maximum in-cloud supersaturation. Only aerosols larger than the cutoff size are incorporated into the cloud water and therefore only these larger particles have the potential to accumulate more sulfate due to aqueous-phase chemistry. For the conditions considered

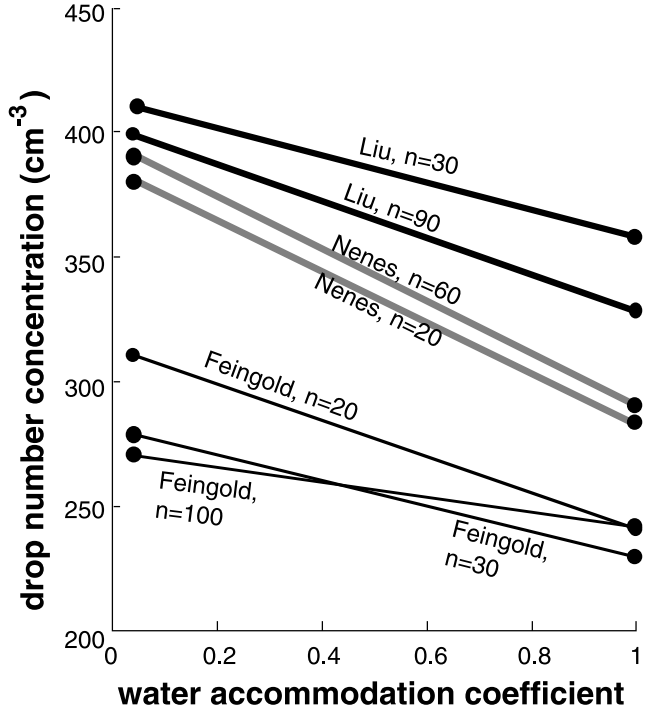

Figure 5. Dependence of computed drop number concentration on water condensation mass accommodation coefficient.

here, Figure 2 shows that the size-resolved models calculated that SO_2 oxidation increased total sulfate aerosol mass by 170–180 ppt from the initial 2 $\mu g\ m^{-3}$ (520 ppt), which represents a 33–35% increase in sulfate mass.

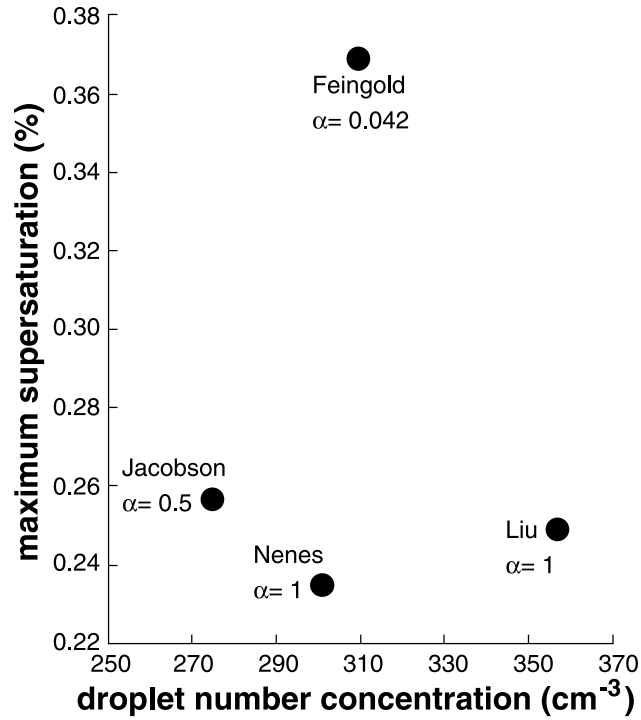

Figure 6. Relationship between maximum supersaturation predicted by the models and droplet number concentration. The value of water condensation mass accommodation coefficient is shown next to the data points.

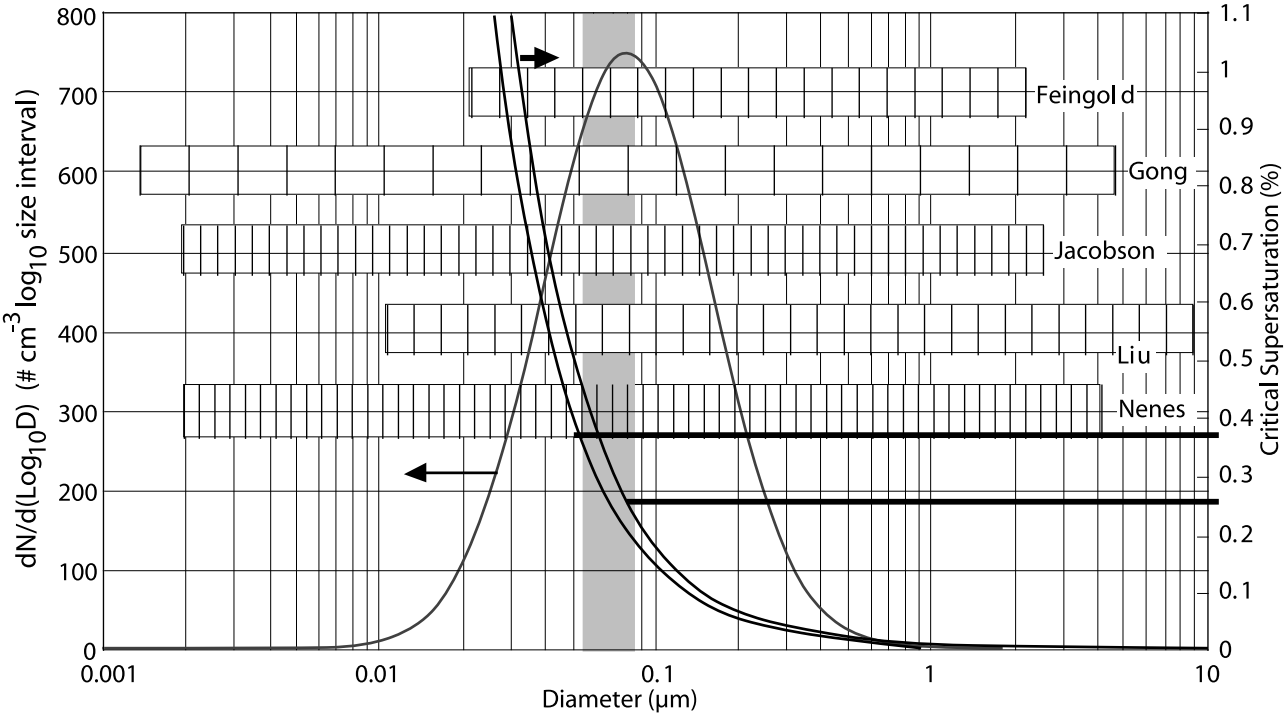

Figure 7. Superposition of initial dry aerosol number distribution, estimated critical supersaturation (Sc) as a function of particle size, and grid structure of the five size-resolved models, shown as "bin" endpoints. The shaded area indicates the size range spanned by the upper and lower estimates of critical supersaturation, according to whether $\nu = 2$ or $\nu = 3$ is assumed in the Köhler equation. The heavy horizontal lines show the largest and smallest maximum supersaturations computed by the five models, and define the width of the shaded area.

[24] In Figure 9, aerosol size distributions are plotted on logarithmic scales (top) and linear scales (bottom) for each model, since each plotting method shows different pertinent details of the changes to the initial spectrum. Figures 9a–9e are sorted in order of increasing number of cloud drops formed at cloud base. All models calculate essentially negligible changes to the larger portion of the aerosol spectra, since the relatively small amount of added sulfate mass does not appreciably modify the diameter of the larger particles. Particles that are smaller than the smallest particle activated are also largely unmodified by cloud chemical processes, since either chemistry in unactivated particles is neglected, or only extremely small amounts of aqueous-phase sulfate formation are calculated within the small size bins.

[25] Particles equal to and larger than the smallest particle activated show the largest increases in particle size due to the mass addition, creating a "minimum" in the processed aerosol spectrum [*Hoppel et al.*, 1990; *Yuen et al.*, 1994; *Hoppel et al.*, 1994]. For the updraft speed, humidity conditions, aerosol composition, and initial size distribution used in this study, the smallest dry diameter activated ranges from 0.06–0.07 μm, in agreement with the range of maximum supersaturations shown in Figure 7. The minimum is less pronounced in the Gong model, because in that model the grown particles are re-mapped onto the original grid, creating some loss of resolution, whereas the other modelers report the grown sizes for the moving discrete points and a modified grid is constructed from that infor-

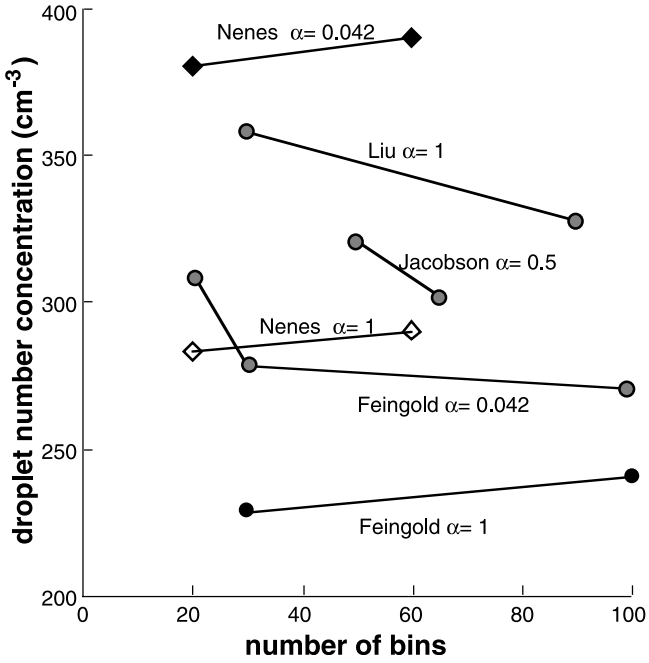

Figure 8. Variation of drop number concentration with number of sizes ("bins"). Applied values of water condensation mass accommodation coefficient are shown alongside each name.

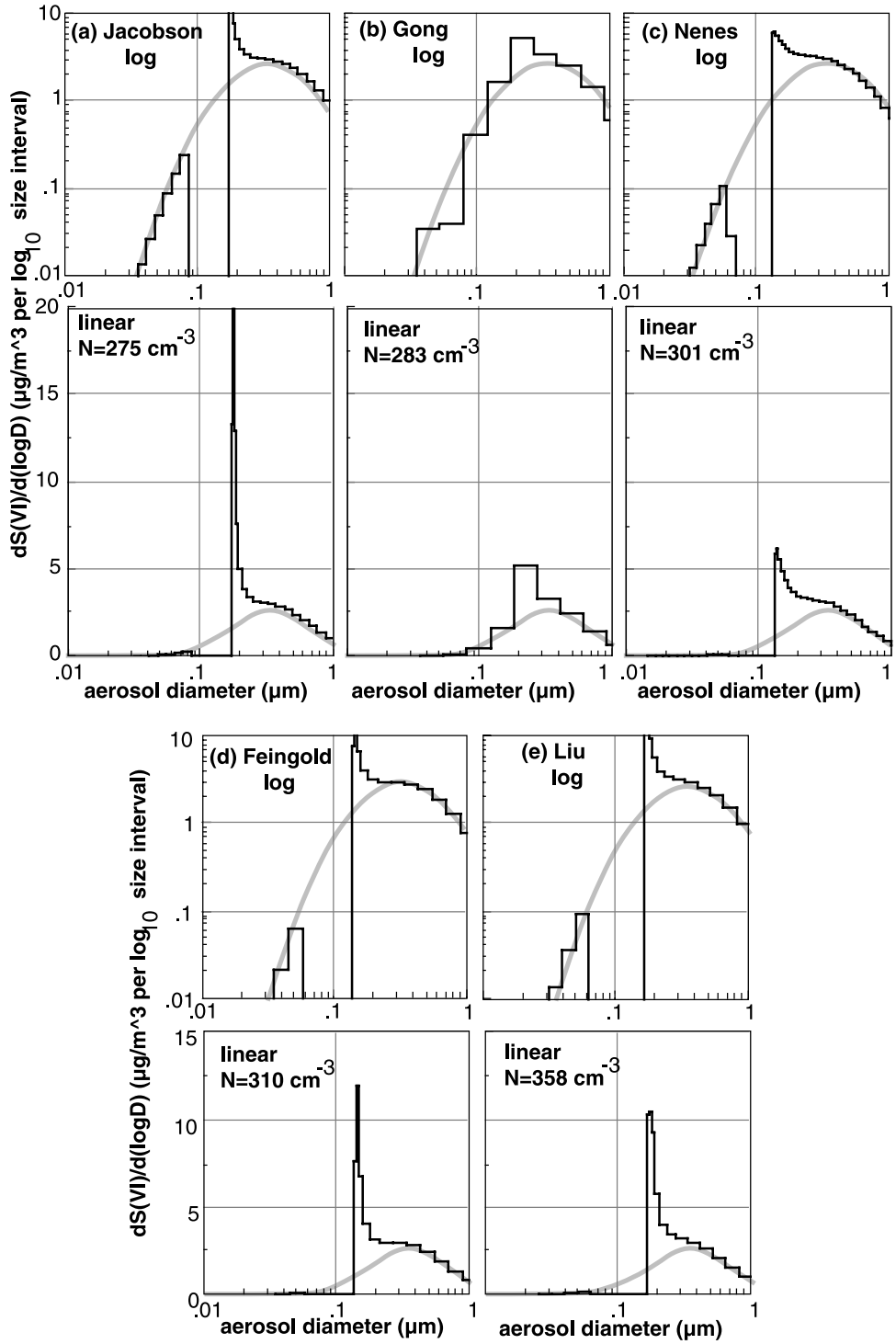

Figure 9. Modification of the dry aerosol sulfate mass distribution according to the five size-resolved models listed in Table 1. Distributions plotted on a log (top) and linear (bottom) scales. Gray curve shows initial input aerosol mass spectrum. Number of cloud drops formed is shown in the lower linear panel of each figure.

mation. The Jacobson and Gong models, forming the fewest number of cloud drops, show significant aerosol mass depletion near aerosol diameters ~0.08–0.12 μm, and increases in the mass concentration distribution in the size range from 0.2–0.3 μm diameter. In contrast, Liu's model, forming the greatest number of cloud drops (358 cm^{-3}), induces appreciable mass concentration depletions down to 0.06 μm diameter, and aerosol mass increases primarily in the 0.15–0.2 μm diameter range.

6. Potential Radiative Effects

[26] In this study, the largest discrepancies among the size-resolved models are the 25–30% differences in the calculated

number of cloud drops formed. These differences will induce appreciable microphysical and radiative impacts [e.g., *Feingold and Kreidenweis*, 2000; *Hegg et al.*, 1996]. Here we crudely estimate the potential direct and indirect radiative impacts. We emphasize that although the relationships between variations in processed aerosol spectra, cloud drop number concentrations, and radiative properties have been explored in many previous studies, some of which are cited earlier, our focus in this work is to examine how differences arising from models treating an identical, simple case propagate into uncertainties in estimates of such relationships.

6.1. Indirect Radiative Effects

[27] Indirect radiative impacts of aerosols refer to the influence of aerosols on the radiative properties of clouds forming on aerosols. To examine the potential impact of model differences on indirect aerosol forcing, we consider the simple *Twomey* [1991] model as summarized by *Seinfeld and Pandis* [1998]. This model proposes that cloud optical depth is proportional to cloud depth, cloud liquid water content to the 2/3 power, and cloud drop number concentration to the 1/3 power. Therefore the range in cloud droplet number calculated in this study (275–358 drops cm^{-3}) translates into approximately a 9% range $[(358/275)^{1/3} - 1]$ in calculated cloud optical depth.

[28] *Twomey*'s [1991] definition of the susceptibility, dR_c/dN, at constant liquid water content, shows that the cloud albedo, R_c, for optically thin clouds is most sensitive to changes in drop number concentration when cloud albedo is 0.5. Under these conditions the approximation $\Delta R_c \approx 0.075 \Delta \ln(N)$ is valid. Using this expression, the 25–30% spread in the calculated droplet number translates into an albedo change of 0.02 [= 0.075ln(358/275)], which is a significant uncertainty in the influence of clouds on the atmospheric energy budget in cloudy areas.

6.2. Direct Radiative Effects

[29] Direct radiative impacts of aerosols refer to the scattering and absorption of light as it passes through an aerosol-laden atmosphere. Here we examine changes in the light scattering properties of the aerosol distributions shown in Figure 9 caused by the addition of sulfate mass by calculating radiative extinction efficiencies from the size distributions.

[30] For this extinction calculation, sulfate is assumed to be associated with ammonium bisulfate aerosol having a refractive index of 1.5, no absorption, and a dry particle density ρ of 1.8 g cm^{-3}. The extinction efficiencies computed for each size distribution are normalized by the mass concentration of ammonium bisulfate aerosol. The single particle light extinction efficiency was calculated for a representative visible wavelength (530 nm) using a Mie theory model of light absorption and scattering by spherical particles [*Bohren and Huffman*, 1983]. Integrations are performed by numerically summing particle diameter "bins" of the size-resolved models, assuming each "bin" is represented by its midpoint diameter.

[31] Figure 10 shows the changes to the extinction efficiency induced by the addition of sulfate mass to the initial distribution by in-cloud SO_2 chemistry. Extinction efficiencies are calculated for dry particles, and for those same particles under high humidity conditions (RH = ~90%), where the particles absorb water and swell in size and mass relative to the dry particles. Recall that all models calculate 34% sulfate mass increases from 520 ppt to 690–700 ppt. However, since the models calculate different number concentrations of droplets, the particle diameters experiencing the most significant growth by mass addition change from model to model.

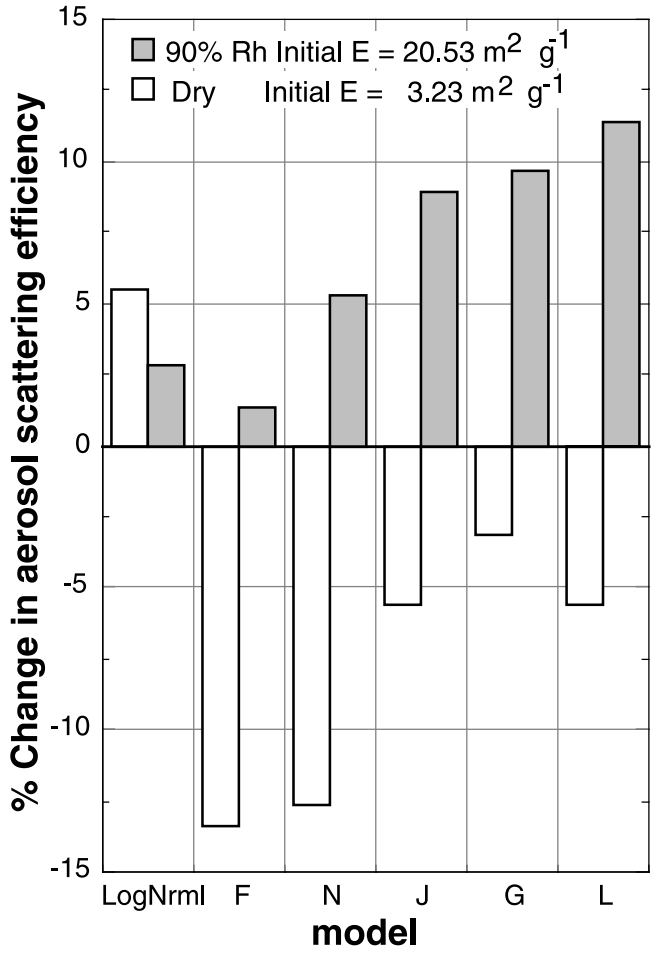

Figure 10. Change in aerosol radiative extinction efficiencies under dry and humidified conditions due to the addition of sulfate mass to the initial lognormal aerosol. Letters along horizontal axis refers to first initial of model name identified in Table 1. Scattering calculation uses the size distributions shown in Figure 9. "LogNrml" model assumes additional mass on lognormal distribution.

[32] Under dry conditions, the initial dry lognormal aerosol distribution is calculated to have an extinction efficiency E = 3.23 m^2 g^{-1}. According to all of the size-resolving models, the addition of sulfate mass under dry conditions decreases the normalized extinction efficiency. This effect results from the fact that all models add sulfate mass to aerosols in the 0.15–0.3 μm diameter range, which is smaller than the aerosol diameter that most efficiently scatters visible radiation (~0.7 μm diameter). The magnitude of this decrease ranges from less than 5% to about 13% relative to the initial lognormal distribution.

[33] Under humid conditions, a wet-to-dry particle diameter ratio of 1.8 is assumed, a reasonable approximation for ammonium bisulfate aerosol at 90% RH [*Tang and Munkelwitz*, 1994]. The initial and final size distributions are

shifted by this factor, and the aerosol mass is increased by the corresponding amount of water required to increase the diameter by 1.8. The computed extinction efficiencies are again normalized by the dry ammonium bisulfate mass. The initial humidified lognormal size distribution now has E = 20.5 m^2 g^{-1}, and all of the modified size distributions show 1–11% increases over this value of E. Under higher humidity conditions, the peak in the sulfate mass distribution is shifted into more optically active diameter ranges.

[34] In Figure 10 one additional simplified calculation (labeled ''LogNrml'') is included. In this case, the additional sulfate mass is uniformly added to the initial distribution in a manner that preserves the lognormal shape of the mass distribution. Such simplifications are often employed in larger-scale models where an aerosol size distribution shape is assumed. The extinction efficiencies computed under this assumption increase under both dry and humid conditions, since mass is added to all particle sizes including those particles that are in the size range of high extinction efficiency. Clearly the assumption of a fixed aerosol size distribution shape limits the ability to accurately characterize radiative impacts associated with changes in mass of the aerosol distribution; in this study, even the sign of the changes in the extinction properties could not be reproduced. This dependence of the scattering efficiency of secondary sulfate on the initial aerosol spectrum, and on the mechanism producing the sulfate, has been pointed out by a number of authors [e.g., *Lelieveld and Heintzenberg*, 1992; *Hegg et al.*, 1993; *Tang*, 1996; *Hegg et al.*, 1996]. Here, we have shown that model-to-model variations for a simple case study, for which all models predicted similar total sulfate formation, can also contribute to variations in computed scattering efficiencies.

7. Conclusions

[35] Larger-scale atmospheric chemistry models that include the formation of sulfate usually use a simplified ''bulk'' approach to account for aqueous-phase SO_2 oxidation. Results for the simple case simulated here indicate a 15–25% difference in the calculated sulfate formation between bulk and size resolving models. These findings are in agreement with prior measurement and modeling work that showed that there is considerable uncertainty introduced in quantifying the oxidation of SO_2 by ozone, induced by pH variations among different cloud drops [*Collett et al.*, 1994; *Reilly et al.*, 2001; *Pandis et al.*, 1990; *Gurciullo and Pandis*, 1997; *Yuen et al.*, 1996; *Zhang et al.*, 1999]. This study extends this analysis to explore differences among modeling approaches as an element of the total uncertainty. Among models of the same type (bulk or size-resolved), the <4% differences in total SO_2-to-sulfate conversion are not very large and would certainly be acceptable in estimates of the contribution of aqueous-phase chemistry to the global sulfur cycle. For the conditions considered here, the underestimate of the $SO_2 + O_3$ reaction induces only a minor change in total sulfate formation despite a factor of 3 underestimate of the $SO_2 + O_3$ contribution. Under other atmospheric conditions, the O_3 reaction may be much more important than in this study.

[36] Detailed analysis of the size-resolved aerosol/cloud chemistry models suggests appreciable uncertainty in the number of dry aerosols that are scavenged in a cloud updraft, even for the relatively simple ammonium bisulfate aerosol distribution considered here. All models calculate approximately consistent and high scavenging of the input dry aerosol mass, but the calculated number of cloud drops formed varies from 275–358 drops cm^{-3}. These differences were found to depend on different treatment of uptake of gases, assumptions regarding solution water content, and different values of water condensation mass accommodation coefficient. Among these, the value of the water condensation mass accommodation coefficient appears to be the single largest source of uncertainty that could be addressed experimentally; in a recent study, *Shaw and Lamb* [1999] report a value of 0.05 as the best fit to their data. Another important factor is the model resolution in diameter space, especially in the critical size range near the smallest particles activated, which is generally not known a priori from updraft and dry aerosol size distribution information. Finally, unlike the conditions chosen for this study, the composition of ambient aerosol is extremely variable, and is an additional source of uncertainty in N_D. It is most likely the largest source of uncertainty in regions affected by anthropogenic pollution, where particles are not as hygroscopic as in more pristine regions.

[37] Using a simple model of cloud radiative properties, the cloud drop number deviations among models were estimated to induce a 9% change in calculated cloud optical depths, and a corresponding change in absolute cloud albedo of up to 2%. For optically thin clouds, this represents an appreciable relative change in cloud albedo. Furthermore, such discrepancies arising in a simple parcel model with well-characterized aerosol composition suggest that radiative and microphysical processes within clouds are highly uncertain within more complex atmospheric cloud models, regional-scale meteorological models, and longer-term climate models where many factors in addition to the uncertainties shown here can arise.

[38] The direct radiative effects of aerosols are also sensitive to how mass is added to an initial aerosol spectrum. Using a simple extinction calculation, we show that the changes to the radiative extinction efficiency, relevant to direct aerosol radiative forcing estimates, can be as large as 13% among model simulations of the same case.

[39] The simulation carried out in this study is inherently limited in scope. Only a single chemical and aerosol condition is specified, with one updraft velocity and vertical displacement. Clearly more general conclusions can only be arrived at with a much wider range of physical and chemical conditions. Variations such as polluted versus clean, oxidant limited versus oxidant rich, overall acidity level and updraft speed are all factors that will influence the results presented here. However, a key factor regulating the magnitudes of the differences found is the relatively large variation in absolute number of cloud drops formed. This discrepancy would probably occur under many environmental conditions, given the reasons leading to it that were diagnosed from this study. This work suggests that an important next step in a cloud-aerosol model comparison series would be a more focused study of the cloud drop activation behavior in the lowest few tens of meters above cloud base in a cloud updraft.

[40] **Acknowledgments.** The authors thank two anonymous reviewers for helpful comments which greatly improved the manuscript. S. K. and G. F. acknowledge support of NOAA Office of Global Programs grants NA67RJ0152 and NA17RJ1228. A. N. acknowledges the support of Office of Naval Research grant N00014-96-1-0119. C. W. acknowledges the U.S. Environmental Protection Agency (EPA) for support under grant R82792901. M. J. acknowledges support from the National Science Foundation (grant ATM 0101596), National Aeronautics and Space Administration (grant NAG5-8645) and the EPA.

References

Ayers, G. P., and T. V. Larson, Numerical study of droplet size dependent chemistry in oceanic, wintertime stratus cloud at southern mid-latitudes, *J. Atmos. Chem.*, *11*, 143–167, 1990.

Barth, M. C., P. J. Rasch, J. T. Kiehl, C. M. Benkovitz, and S. E. Schwartz, Sulfur chemistry in the National Center for Atmospheric Research Community Climate Model: Description, evaluation, features and sensitivity to aqueous chemistry, *J. Geophys. Res.*, *105*, 1387–1415, 2000.

Bohren, C. F., and D. R. Huffman, Absorption and scattering of light by small particles, 544 pp., John Wiley, New York, 1983.

Boucher, O., and U. Lohmann, The sulfate-CCN-cloud albedo effect, *Tellus, Ser. B*, *47*, 281–300, 1995.

Chang, J. S., R. A. Brost, I. S. A. Isaksen, S. Madronich, P. Middleton, W. R. Stockwell, and C. J. Walcek, A three-dimensional Eulerian acid deposition model: Physical concepts and formulation, *J. Geophys. Res.*, *92*, 14,681–14,700, 1987.

Collett, J. L., Jr., A. Bator, X. Rao, and B. Demoz, Acidity variations across the cloud drop size spectrum and their influence on rates of atmospheric sulfate production, *Geophys. Res. Lett.*, *21*, 2393–2396, 1994.

Feingold, G., and S. M. Kreidenweis, Does cloud processing of aerosol enhance droplet concentrations, *J. Geophys. Res.*, *105*, 24,351–24,361, 2000.

Feingold, G., S. M. Kreidenweis, and Y. Zhang, Stratocumulus processing of gases and cloud condensation nuclei, part I, Trajectory ensemble model, *J. Geophys. Res.*, *103*, 19,527–19,542, 1998.

Gong, W., Modelling cloud chemistry in a regional aerosol model: Bulk vs. size resolved representation, in *Air Pollution Modeling and Its Applications*, vol. 15, edited by C. Borrego and G. Schayes, pp. 285–293, Plenum, New York, 2002.

Gurciullo, C. S., and S. N. Pandis, Effect of composition variations in cloud droplet populations on aqueous-phase chemistry, *J. Geophys. Res*, *102*, 9375–9385, 1997.

Health Effects Institute, Reanalysis of the Harvard Six Cities Study and the American Cancer Society Study of particulate air pollution and mortality, Health Effects Inst. spec. rep., Cambridge, Mass., July 2000 (available at http://www.healtheffects.org/pubs-special.htm).

Hegg, D. A., Cloud condensation nucleus-sulfate mass relationship and cloud albedo, *J. Geophys. Res.*, *99*, 25,903–25,907, 1994.

Hegg, D. A., and T. V. Larson, The effects of microphysical parameterization on model predictions of sulfate production in clouds, *Tellus, Ser. B*, *42*, 272–284, 1990.

Hegg, D. A., P. F. Yuen, and T. V. Larson, Modeling the effects of heterogeneous cloud chemistry on the marine particle size distribution, *J. Geophys. Res.*, *97*, 12,927–12,933, 1992.

Hegg, D., T. Larson, and P. F. Yuen, A theoretical study of the effect of relative humidity on light scattering by tropospheric aerosols, *J. Geophys. Res.*, *98*, 18,435–18,439, 1993.

Hegg, D. A., R. Majeed, P. F. Yuen, M. B. Baker, and T. V. Larson, The impacts of SO_2 oxidation in cloud drops and in haze particles on aerosol light scattering and CCN activity, *Geophys. Res. Lett.*, *23*, 2613–2616, 1996.

Hoppel, W. A., J. W. Fitzgerald, G. M. Frick, and R. E. Larson, Aerosol size distributions and optical properties found in the marine boundary layer over the Atlantic Ocean, *J. Geophys. Res.*, *95*, 3659–3686, 1990.

Hoppel, W. A., G. M. Frick, J. W. Fitzgerald, and B. J. Wattle, A cloud chamber study of the effect that nonprecipitating water clouds have on the aerosol-size distribution, *Aerosol Sci. Technol.*, *20*(1), 1–30, 1994.

Intergovernmental Panel on Climate Change, Third assessment report, technical summary, IPCC Secr., World Meteorol. Org., Geneva, Switzerland, 2001.

Iribarne, J. V., and H. R. Cho, Models of cloud chemistry, *Tellus, Ser. B*, *41*, 2–23, 1989.

Jacobson, M. Z., Analysis of aerosol interactions with numerical techniques for solving coagulation, nucleation, condensation, dissolution, and reversible chemistry among multiple size distributions, *J. Geophys. Res.*, *107*(D19), 4366, doi:10.1029/2001JD002044, 2002.

Jones, A., D. L. Roberts, and A. Slingo, A climate model study of indirect radiative forcing by anthropogenic sulfate aerosols, *Nature*, *370*, 450–453, 1994.

Kim, C.-H., S. M. Kreidenweis, G. Feingold, G. J. Frost, and M. K. Trainer, Modeling cloud effects on hydrogen peroxide and methylhydroperoxide in the marine atmosphere, *J. Geophys. Res*, *107*(D2), 4018, doi:10.1029/2000JD000285, 2002.

Lelieveld, J., and J. Heintzenberg, Sulfate cooling effect on climate through in-cloud oxidation of anthropogenic SO_2, *Science*, *258*, 117–120, 1992.

Liu, X., and W. Seidl, Modeling study of cloud droplet nucleation and in-cloud sulfate production during the SANA 2 Campaign, *J. Geophys. Res*, *103*, 16,145–16,158, 1998.

Malm, W. C., J. F. Sisler, D. Huffman, R. A. Eldred, and T. A. Cahill, Spatial and seasonal trends in particle concentration and optical extinction in the United States, *J. Geophys. Res.*, *99*, 1347–1370, 1994.

Nenes, A., S. Gahn, H. Abdul-Razzak, P. Y. Chuang, and J. H. Seinfeld, Kinetic limitations on cloud droplet formation and impact on cloud albedo, *Tellus, Ser. B*, *53*, 133–149, 2001.

Ogren, J. A., and R. J. Charlson, Implications for models and measurements of chemical inhomogeneities among cloud droplets, *Tellus, Ser. B*, *44*, 208–225, 1992.

Pandis, S. N., J. H. Seinfeld, and C. Pilinis, Chemical composition differences in fog and cloud droplets of different sizes, *Atmos. Environ., Part A*, *24*, 1957–1969, 1990.

Rasch, P. J., M. C. Barth, J. T. Kiehl, S. E. Schwartz, and C. M. Benkovitz, A description of the global sulfur cycle and its controlling processes in the National Center for Atmospheric Research Community Climate Model Version 3, *J. Geophys. Res.*, *105*, 1367–1385, 2000.

Reilly, J. E., O. V. Rattigan, K. F. Moore, C. Judd, D. E. Sherman, V. A. Dutkiewicz, S. M. Kreidenweis, L. Husain, and J. L. Collett Jr., Drop size-dependent S(IV) oxidation in chemically heterogeneous California radiation fogs, *Atmos. Environ.*, *35*, 5717–5728, 2001.

Seidl, W., Ionic concentrations and initial S(IV) oxidation rates in droplets during the condensational stage of cloud, *Tellus, Ser. B*, *41*, 32–50, 1989.

Seinfeld, J. H., and S. N. Pandis, *Atmospheric Chemistry and Physics*, 1326 pp., Wiley-Interscience, New York, 1998.

Shaw, R. A., and D. Lamb, Experimental determination of the thermal accommodation and condensation coefficients of water, *J. Chem. Phys.*, *111*, 10,659–10,663, 1999.

Stockwell, W. R., P. Middeleton, J. S. Chang, and X. Tang, The second generation regional acid deposition model chemical mechanism for regional air quality modeling, *J. Geophys. Res.*, *95*, 16,343–16,367, 1990.

Tang, I. N., Chemical and size effects of hygroscopic aerosols on light scattering coefficients, *J. Geophys. Res.*, *101*, 19,245–19,250, 1996.

Tang, I. N., and H. R. Munkelwitz, Water activities, densities, and refractive indices of aqueous sulfates and sodium nitrate droplets of atmospheric importance, *J. Geophys. Res.*, *99*, 18,801–18,808, 1994.

Twomey, S., Aerosols, clouds and radiation, *Atmos. Environ, Part A*, *25*, 2435–2442, 1991.

Walcek, C. J., and G. Taylor, A theoretical method for computing vertical distributions of acidity and sulfate production within cumulus clouds, *J. Atmos. Sci.*, *43*, 339–355, 1986.

Yuen, P.-F., D. A. Hegg, and T. V. Larson, The effects of in-cloud sulfate production on light-scattering properties of continental aerosol, *J. Appl. Meteorol.*, *33*, 848–854, 1994.

Yuen, P.-F., D. A. Hegg, T. V. Larson, and M. C. Barth, Parameterization of heterogeneous droplet chemistry for use in bulk cloud models, *J. Appl. Meteorol.*, *35*, 679–689, 1996.

Zhang, Y., S. M. Kreidenweis, and G. Feingold, Stratocumulus processing of gases and cloud condensation nuclei, 2, Chemistry sensitivity analyses, *J. Geophys. Res.*, *104*, 16,061–16,080, 1999.

G. Feingold, National Oceanographic and Atmospheric Administration, 325 Broadway, Boulder, CO 80305, USA.

W. Gong, Meteorological Service of Canada, 4905 Dufferin Street, Downsview, Ontario, Canada M3H 5T4.

M. Z. Jacobson, Department of Civil and Environmental Engineering, Stanford University, Terman Engineering Center, Room M-13, Stanford, CA 94305-4020, USA.

C.-H. Kim, National Institute of Environmental Research (NIER), Kyong-Seo-dong, 2-1, Seo-gu, Incheon 404-170, Korea.

S. M. Kreidenweis, Department of Atmospheric Science, Colorado State University, Fort Collins, CO 80523, USA. (sonia@chem.atmos.colostate.edu)

X. Liu and J. E. Penner, Atmospheric, Oceanic and Space Sciences, University of Michigan, 2455 Hayward, Ann Arbor, MI 48109-1349, USA.

A. Nenes, School of Earth and Atmospheric Sciences, Georgia Institute of Technology, Atlanta, GA 30332-0340, USA.

J. H. Seinfeld, Division of Chemistry and Chemical Engineering, 210-41, California Institute of Technology, 1200 E. California Blvd., Pasadena, CA 91125, USA.

C. J. Walcek, Atmospheric Science Research Center, State University of New York, 251 Fuller Road, Albany, NY 12203, USA. (walcek@asrc.cestm.albany.edu)